Electronic Supplementary Information (ESI)

Light-Regulating Chirality of Metallacages Featuring Dithienylethene Switches

Shaomeng Guo,[‡] Mengqi Li,[‡] Honglong Hu, Ting Xu, Hancheng Xi, and Wei-Hong Zhu*

Key Laboratory for Advanced Materials and Joint International Research Laboratory of Precision Chemistry, Molecular Engineering Feringa Nobel Prize Scientist Joint Research Center, Shanghai Key Laboratory of Functional Materials Chemistry, Institute of Fine Chemicals, School of Chemistry and Molecular Engineering, East China University of Science and Technology, 200237, China. E-mail: whzhu@ecust.edu.cn

Contents

1. General

All starting reagents were commercially available without further treatment. Solvents used were analytical grade without further treatment, except those for recrystallization and optical tests, which were purified by distillation. All NMR spectra were recorded on Bruker AM-400 and Bruker AM-600 spectrometers with tetramethyl silane as an internal reference, where CD_3CN and $CDCl_3$ were used as solvents. High resolution mass (HRMS) spectra were recorded on a Waters LCT Premier XE spectrometer with acetonitrile as solvent. Absorption spectra were recorded on Agilent Cary 60 (1cm quartz cell). The photochromic reaction was induced in situ by continuous irradiation using an Hg/Xe lamp (Hamamatsu, LC8 Lightningcure, 200 W) equipped with a narrow band interference filter (Shenyang HB optical Technology) for $\lambda_{irr} = 313 \pm 10$ nm, a broad band interference filters (Shenyang HB optical Technology) for $\lambda_{irr} > 510$ nm, or a monochromator (monoscan 2000, OceanOptics) for $\lambda_{irr} = 515 \pm 10$ nm. The photochromic reaction quantum yields for photocyclization and cycloreversion were measured by the standard procedures using BTF6 as the reference. The rates of isomerization in the initial stage of the reaction (0-3%) were compared with references, whose Φ_{o-c} (35%) and Φ_{c-o} (35%) in hexane, which brought for the 3% uncertainties on the calculations of quantum yields. Fourier transform infrared (FT-IR) spectra were recorded on a JASCO model FT-IR-6100 infrared spectrometer. The temperature-dependent CD spectra were recorded using JASCO J-810 spectropolarimeter connecting a thermostatic bath.
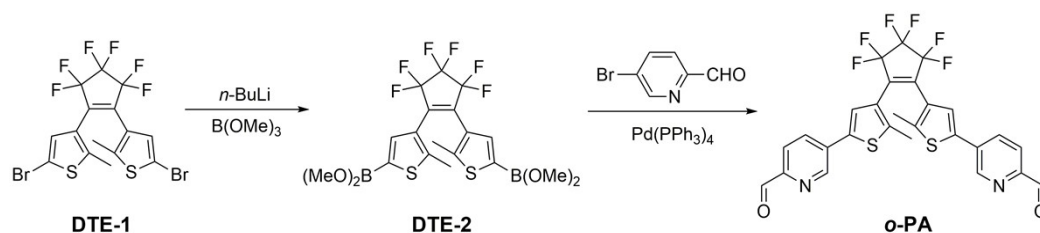
2. Synthetic details

Compound **DTE-1** was prepared according to the established methods.[1]
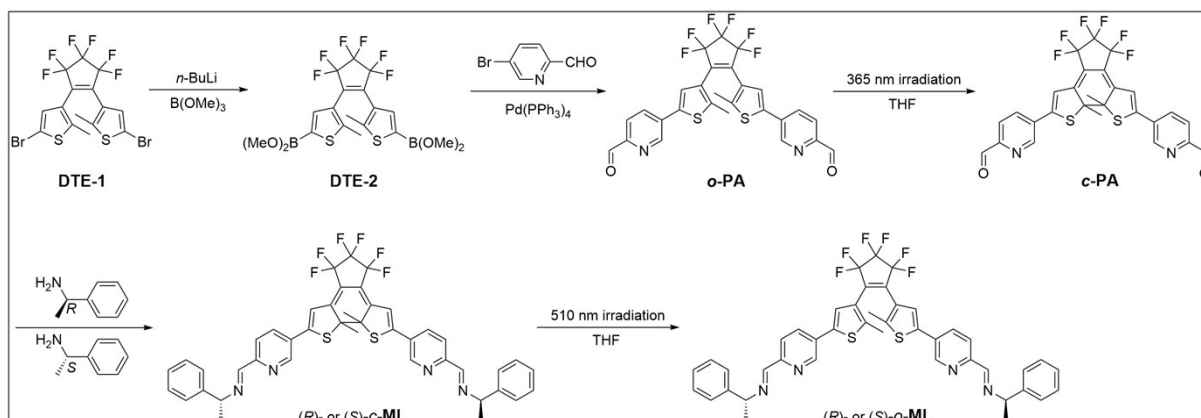
Scheme S1. Synthetic route of *o*/*c*-**PA**, (*R*)/(*S*)-*o*-**ML** and (*R*)/(*S*)-*c*-**ML**

2.1 Synthesis of ligand *o*-PA

The hexane solution of *n*-BuLi (4.1 mL, 6.56 mmol) was added dropwise at -75 °C under N_2 atmosphere to a solution of compound **DTE-1** (1.57 g, 3.0 mmol) in anhydrous THF (30 mL). The colour of solution turned to brown black. After 45 min, tributyl borate (1 mL, 9.0 mmol) was added and warmed to room temperature slowly. After stirring for 2 h, the resulting brown black solution of **DTE-2** was used directly for the following reaction. Added 5-bromopicolinaldehyde (1.3 g, 6.3 mmol), 10 mL water solution of K_2CO_3 (2 M) and Pd(PPh$_3$)$_4$ (517.0 mg, 0.45 mmol) to above solution of **DTE-2** under N_2 atmosphere. This reaction system was heated at 75 °C for 12 h. Upon reaction completion, poured the residue into water (50 mL), extracted with dichloromethane (60 mL × 3), the organic phase was collected and evaporated under reduced pressure. The residue was purified by column chromatography (petroleum ether: ethyl acetate = 3/1, *v/v*) to afford *o*-**PA** percussor as yellow power (905.3 mg). Yield, 52%. ^{1}H NMR (400 MHz, CDCl$_3$, 293 K): δ [ppm] 2.06 (s, 6 H, -CH$_3$), 7.48 (s, 2 H, thienyl-H),7.99 (d, *J* = 0.8 Hz, 4 H, pyridyl-H), 8.96 (s, 2 H, pyridyl-H), 10.07 (s, 2 H, -CHO). ^{13}C NMR (100 MHz, CDCl$_3$, 293 K): δ [ppm] 192.51, 151.69, 146.74, 144.32, 137.42, 133.14, 132.96, 126.46, 125.23, 122.01, 14.83. HRMS-ESI (*m/z*): [M + H]$^+$ Calcd. for (C$_{27}$H$_{17}$O$_2$N$_2$F$_6$S$_2$), 579.0630, found: 579.0635.
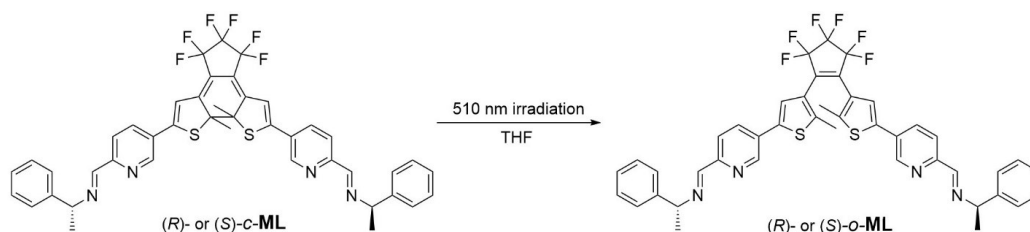
2.2 Synthesis of ligand *c*-PA
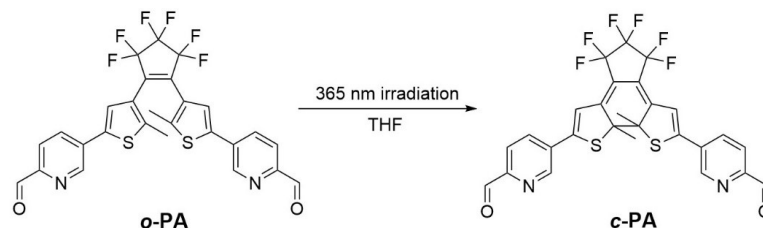
o-PA (290.5 mg, 0.5 mmol) was dissolved in THF (200 mL), and then irradiated with ultraviolet lamps (λ = 365 ± 10 nm) until reaching PSS. After removing the solvent, the residual was purified by column chromatography on silica (dichloromethane) to obtain *c*-PA as blue powder (182.4 mg). Yield, 62.1%. ^{1}H NMR (400 MHz, CDCl$_3$, 293 K): δ [ppm] 2.24 (s, 6 H, -CH$_3$), 6.87 (s, 2 H, thienyl-H),8.02 (d, 4 H, pyridyl-H), 8.97 (s, 2 H, pyridyl-H), 10.10 (s, 2 H, -CHO). ^{13}C NMR (100 MHz, CDCl$_3$, 293 K): δ [ppm] 192.33, 153.61, 153.17, 149.22, 147.99, 134.77, 132.45, 121.50, 117.03, 66.62, 25.33. HRMS-ESI (*m/z*): [M + H]$^+$ Calcd. for (C$_{27}$H$_{17}$O$_2$N$_2$F$_6$S$_2$), 579.0630, found: 579.0637.

2.3 Synthesis of ligand (*R*) or (*S*)-*c*-ML
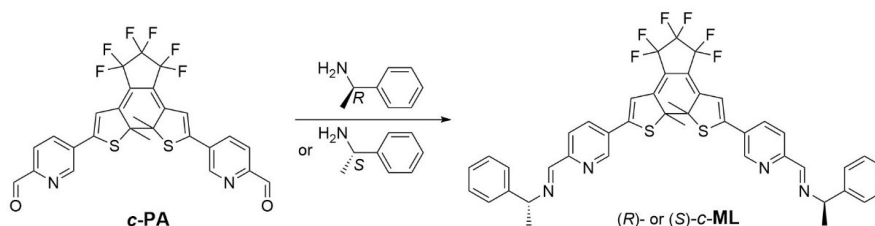
Ligand *c*-PA (30.0 mg, 0.1 mmol, 1 equiv), (*R*)- or (*S*)-1-phenylethylamine (30.3 mg, 0.25 mmol, 2.5 equiv) were added to a flask with 5 mL dry DCM, at 25°C for 12 h led to blue solution. After concentrating DCM solution to 2 mL, then 20 mL hexane solution was used to precipitate the product. Pure (*R*)- or (*S*)-*c*-ML was obtained as a blue solid (35.1 mg). Yield, 44.6%.^{1}H NMR (600 MHz, CDCl$_3$, 293 K): δ [ppm] 1.63 (d, *J* = 6.6 Hz, 6 H, -CH$_3$), 2.21 (s, 6 H, -CH$_3$), 4.68 (d, *J* = 6.0 Hz, 2 H, -CH-), 6.78 (s, 2 H, thienyl-H), 7.27 (d, *J* = 7.2 Hz, 2 H, phenyl-H), 7.36 (dd, *J$_1$* = 7.8 Hz, *J$_2$* = 7.2 Hz, 4 H, phenyl-H), 7.44 (d, 4 H, *J* = 7.2 Hz, phenyl-H), 7.87 (d, 2 H, *J* = 8.4 Hz, pyridyl-H), 8.15 (d, 2 H, *J* = 8.4 Hz, pyridyl-H), 8.47 (s, 2 H, -CH=N), 8.81 (s, 2 H, pyridyl-H). ^{13}C NMR (150 MHz, CDCl$_3$, 293 K): δ [ppm] 159.60, 155.90, 154.18, 149.11, 147.29, 144.24, 134.17, 129.68, 128.59, 127.29, 126.73, 121.30, 115.60, 69.77, 66.45, 25.29, 24.53. HRMS-ESI (*m/z*): [M + H]$^+$ Calcd. for (C$_{43}$H$_{35}$N$_4$F$_6$S$_2$), 785.2207, found: 785.2233.

2.4 Synthesis of ligand (*R*)- or (*S*)-*o*-ML



(*R*)- or (*S*)-*c*-**ML** (200.1 mg, 0.25 mmol) was dissolved in THF (30 mL), and then irradiated with visible light (λ > 510 nm) until reaching PSS. After removing the solvent, the residual was purified by column chromatography on silica (dichloromethane) to obtain (*R*)- or (*S*)-*o*-**ML** as yellow powder (195.2 mg). Yield, 97.5%.^{1}H NMR (400 MHz, CD$_3$CN, 293 K): δ [ppm] 1.57 (d, *J* = 6.8 Hz, 6 H, -CH$_3$), 2.06 (s, 6 H, -CH$_3$), 4.69 (q, *J* = 6.4 Hz, 2 H, -CH-), 7.28 (t, 2 H, *J$_1$* = 7.6 Hz, phenyl-H), 7.38 (dd, *J$_1$* = 8.0 Hz, *J$_2$* = 7.2 Hz, 4 H, phenyl-H), 7.49 (d, *J* = 7.6 Hz, 4 H, phenyl-H), 7.57 (s, 2 H, thienyl-H), 8.01 (dd, 2 H, *J$_1$* = 2.0 Hz, *J$_2$* = 8.0 Hz, pyridyl-H), 8.06 (d, 2 H, *J* = 8.4 Hz, pyridyl-H), 8.48 (s, 2 H, -CH=N), 8.88 (d, *J* = 1.6 Hz, 2 H, pyridyl-H). HRMS-ESI (*m/z*): [M + H]$^+$ Calcd. for (C$_{43}$H$_{35}$N$_4$F$_6$S$_2$), 785.2207, found: 785.2236.

## 2.5 Synthesis of metallacages (*R*)- or (*S*)-*o*-cage
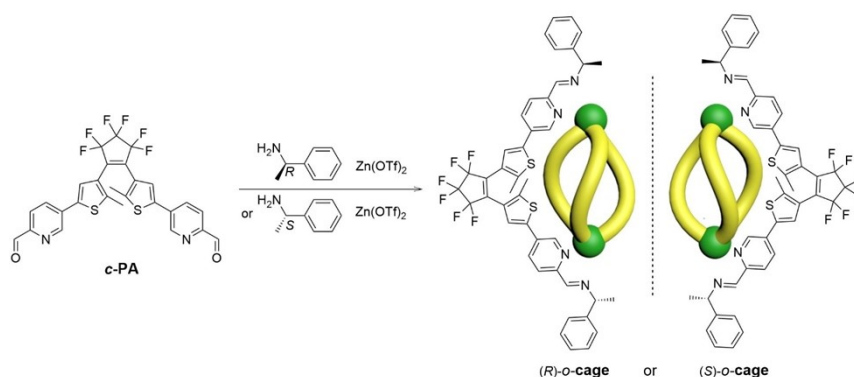
Ligand *o*-**PA** (17.3 mg, 0.03 mmol, 3 equiv), (*R*)- or (*S*)-1-phenylethylamine (7.3 mg, 0.06 mmol, 6 equiv) and zinc triflate (7.3 mg, 0.02 mmol, 2 equiv) were added to a flask with 5 mL acetonitrile solution, then heated at 70 °C for 12 h led to clear yellow solution. After cooling, 20 mL isopropyl ether was used to precipitate the product. Pure (*R*)- or (*S*)-*o*-**cage** was obtained as a yellow solid (25.2 mg). Yield, 82.1%.^{1}H NMR (400 MHz, CD$_3$CN, 293 K): δ [ppm] 1.55 (d, *J* = 2.0 Hz, 18 H, -CH$_3$), 1.77 (s, 18 H, -CH$_3$), 5.52 (d, *J* = 2.4 Hz, 6 H, -CH-), 6.83 (d, *J* = 7.6 Hz, 12 H, phenyl-H), 6.99 (dd, *J$_1$* = 7.6 Hz, *J$_2$* = 7.2 Hz, 12 H, phenyl-H), 7.13 (s, 6 H, pyridyl-H), 7.20 (t, 6 H, *J* = 7.2 Hz, phenyl-H), 7.69 (d, *J* = 8.0 Hz, 6 H, pyridyl-H), 7.85 (s, 6 H, thienyl-H), 8.07 (s, 6 H, -CH=N),8.60 (d, *J* = 8.0 Hz, 6 H, pyridyl-H). ^{13}C NMR (150 MHz, CD$_3$CN, ppm): δ 160.46, 145.60, 144.62, 142.69, 140.84, 136.57, 135.46, 133.58, 130.35, 128.85, 128.80, 127.86, 127.13, 126.28, 126.06, 126.01, 64.53, 22.64, 13.99. HRMS-ESI: *m/z* 877.8164 for [*o*-**cage** - 3OTf]$^{3+}$, *m/z* 1391.1832 for [*o*-**cage** - 2OTf]$^{2+}$.

2.6 Synthesis of metallacages (*R*)- or (*S*)-*c*-cage
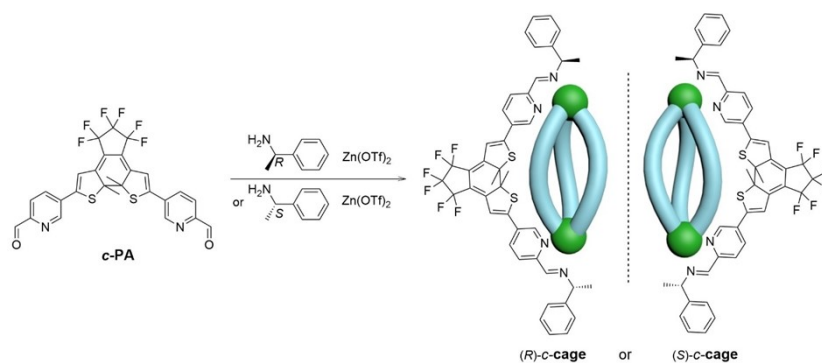
Ligand *c*-**PA** (17.3 mg, 0.03 mmol, 3 equiv), (*R*)- or (*S*)-1-phenylethylamine (7.3 mg, 0.06 mmol, 6 equiv) and zinc triflate (7.3 mg, 0.02 mmol, 2 equiv) were added to a flask with 5 mL acetonitrile solution, at 25°C for 12 h led to blue solution. Upon reaction completion, 20 mL isopropyl ether was used to precipitate the product. Pure (*R*)- or (*S*)-*c*-**cage** was obtained as a blue solid (24.8 mg). Yield, 81.5%.^{1}H NMR (400 MHz, CD$_3$CN, 293 K): δ [ppm]: 1.08 (m, 18 H, -CH$_3$), 1.63-1.79 (m, 18 H, -CH$_3$), 5.52 (m, 6 H, -CH-), 6.65-6.70 (m, 12 H, phenyl-H), 7.01-7.06 (m, 12 H, phenyl-H), 7.21 (m, 6 H, phenyl-H), 7.39-7.42 (m, 6 H, pyridyl-H), 7.47-7.49 (m, 6 H, pyridyl-H), 7.66-7.80 (m, 6 H, thienyl-H), 8.11-8.14 (m, 6 H, pyridyl-H),8.28-8.32 (m, 6 H, -CH=N). **Notes:** Because of the chiral inequality phenomenon, we cannot acquire the ^{13}C NMR spectra of *c*-**cage** by 500 MHz NMR. Therefore, as shown in main text, we adapted an indirect approach to prove the fabrication of *c*-**cage** by taking advantage of the reversible conversion of the inserted BTE.

2.7 Synthesis of achiral metallacages *c*-2 and *o*-2
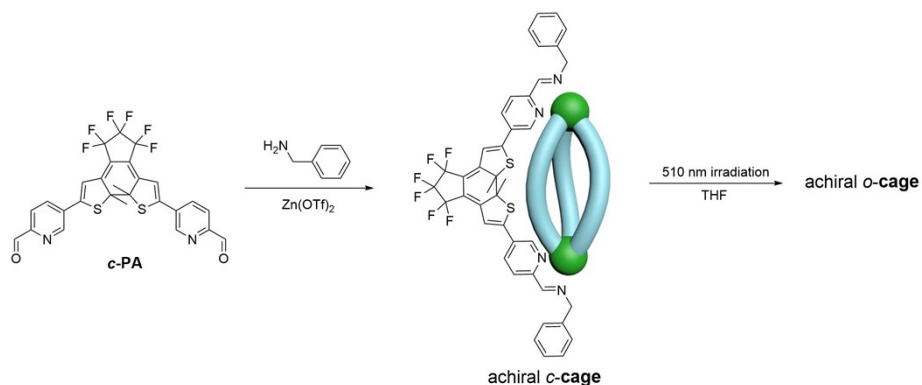
Ligand *c*-**PA** (17.3 mg, 0.03 mmol, 3 equiv), phenylmethylamine (6.4 mg, 0.06 mmol, 6 equiv) and zinc triflate (7.3 mg, 0.02 mmol, 2 equiv) were added to a flask with 5 mL acetonitrile solution, at 25°C for 12 h led to blue solution. Upon reaction completion, 20 mL isopropyl ether was used to precipitate the product, achiral *c*-**cage** was obtained as a blue solid (24.1 mg). Yield, 79.1%. HRMS-ESI: *m/z* 600.1002 for [*c*-**2** - 4OTf]$^{4+}$, *m/z* 849.7842 for [*c*-**2** - 3OTf]$^{3+}$, 1349.1528 for [*c*-**2** - 2OTf]$^{2+}$.

Metallacage *o*-**2**:^{1}H NMR (400 MHz, CD$_3$CN, 293 K): δ [ppm] 1.79 (s, 18 H, -CH$_3$), 1.77 (s, 18 H, -CH$_3$), 4.89 (d, *J* = 14.0 Hz, 6 H, -CH$_2$-), 5.21 (d, *J* = 12.8 Hz, 6 H, -CH$_2$-), 7.00 (d, *J* = 7.2 Hz, 12 H, phenyl-H), 7.09 (t, *J* = 8.0 Hz, 12 H, phenyl-H), 7.27 (t, *J* = 7.2 Hz, 6 H, pyridyl-H), 7.33 (s, 6 H, pyridyl-H), 7.65 (d, *J* = 8.4 Hz, 6 H, phenyl-H), 7.85 (s, 6 H, thienyl-H), 7.99 (s, 6 H, -CH=N),8.57 (q, J_1 = 8.4 Hz, J_2 = 2.0 Hz, 6 H, pyridyl-H). ^{13}C NMR (100 MHz, CD$_3$CN, ppm): δ 163.64, 145.02, 144.35, 142.91, 136.07, 135.09, 134.44, 133.29, 129.61, 128.45, 128.09, 127.61, 126.83, 125.89, 122.43, 119.25, 62.06, 54.01, 13.67. HRMS-ESI: *m/z* 600.1002 for [*o*-**2** - 4OTf]$^{4+}$, *m/z* 848.7867 for [*o*-**2** - 3OTf]$^{3+}$, 1349.1530 for [*o*-**2** - 2OTf]$^{2+}$.

3. Chemical structure characterization of metallacages
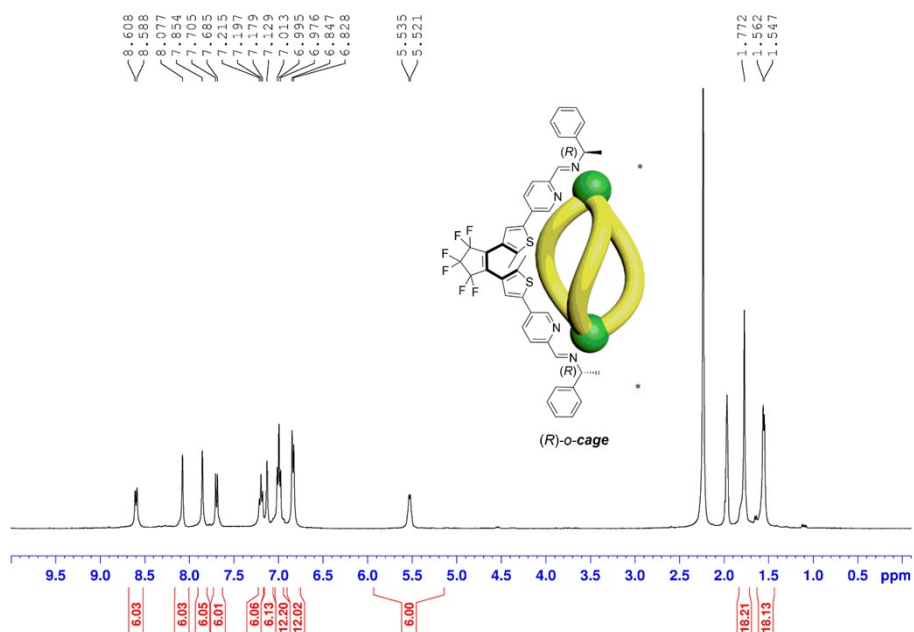
3.1 ¹H NMR spectrum of *o*-cage

Fig. S1 ¹H NMR (400 MHz, CD$_3$CN, 293 K) spectrum of *o*-**cage**.

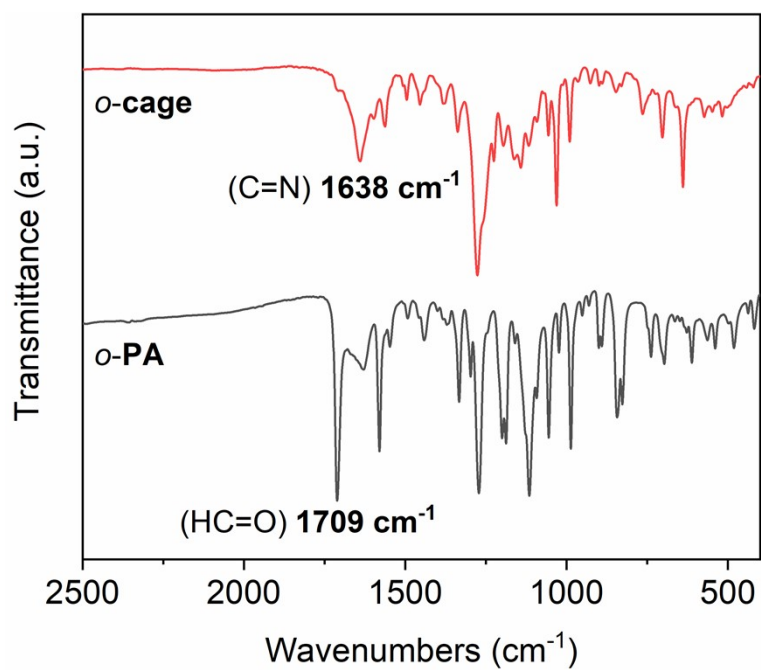## 3.2 FT-IR spectroscopy of *o*-PA and *o*-cage

Fig. S2 FT-IR spectroscopy of *o*-**cage** and *o*-**PA**.

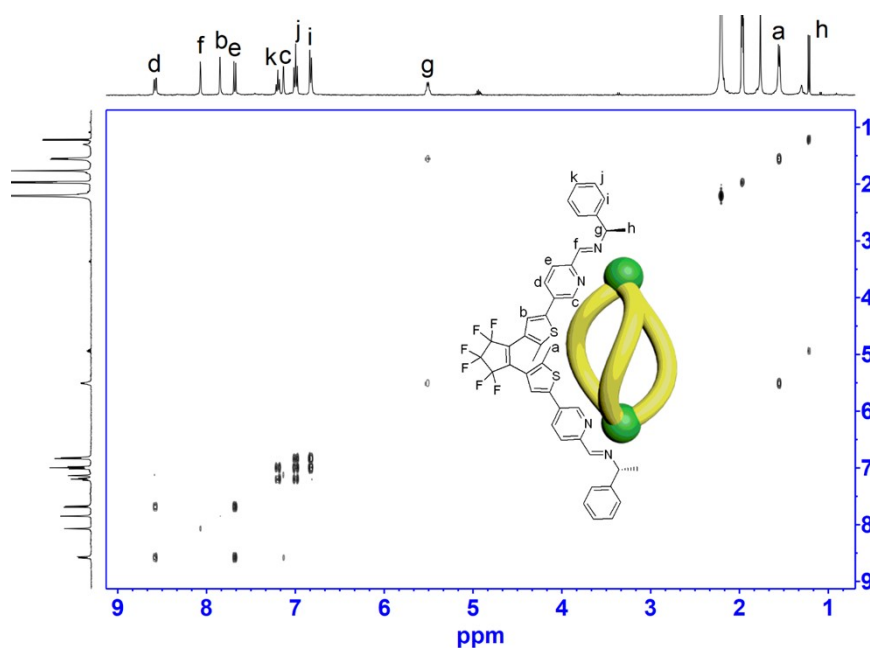## 3.3 ¹H-¹H COSY spectrum of *o*-cage

Fig. S3 ¹H-¹H COSY (400 MHz, CD₃CN, 293 K) spectrum of *o*-**cage**.
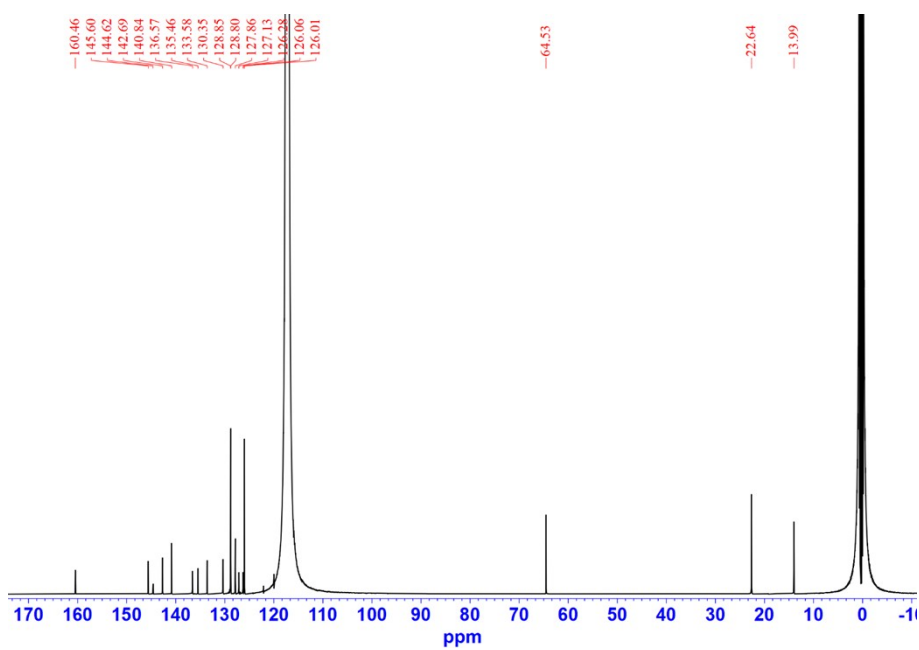
3.4 ¹³C NMR spectrum of *o*-cage

Fig. S4 ¹³C NMR (150 MHz, CD₃CN, 293 K) spectrum of *o*-**cage**.
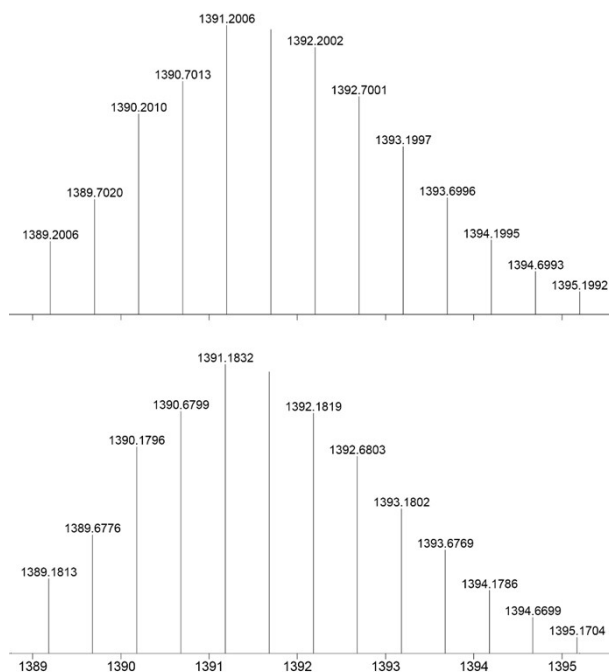
3.5 ESI-HRMS spectra of *o*-cage

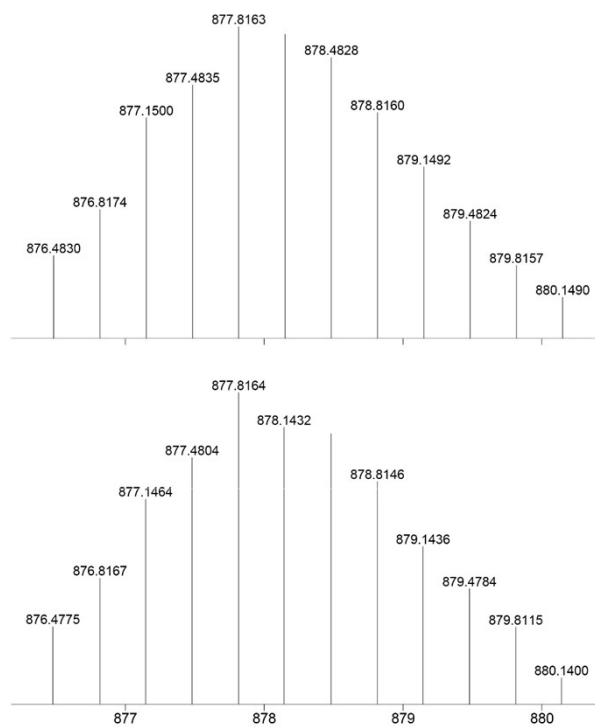**Fig. S5** ESI-HRMS spectrum of *o*-**cage** of [M - 2OTf]$^{2+}$, theoretical (top) and experimental (bottom).

Fig. S6 ESI-HRMS spectrum of *o*-**cage** of [M - 3OTf]$^{3+}$, theoretical (top) and experimental (bottom).
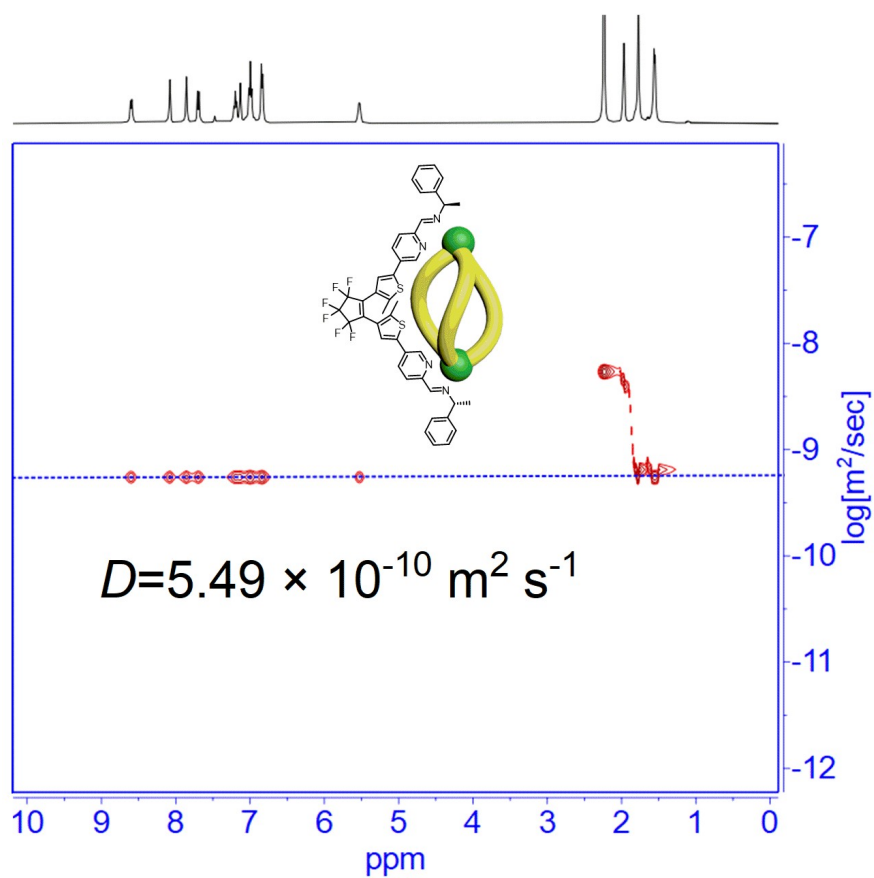
3.6 DOSY spectrum of *o*-cage

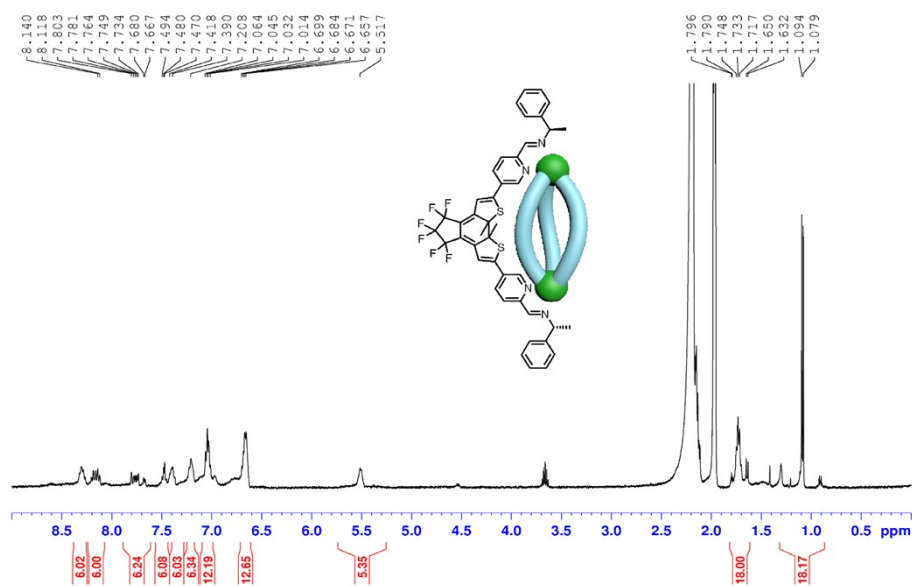**Fig. S7** DOSY spectrum of *o*-**cage**.

3.7 ¹H NMR spectrum of *c*-cage

Fig. S8 ¹H NMR (400 MHz, CD₃CN, 293 K) spectrum of *c*-**cage**.

3.8 DOSY spectrum of *c*-cage

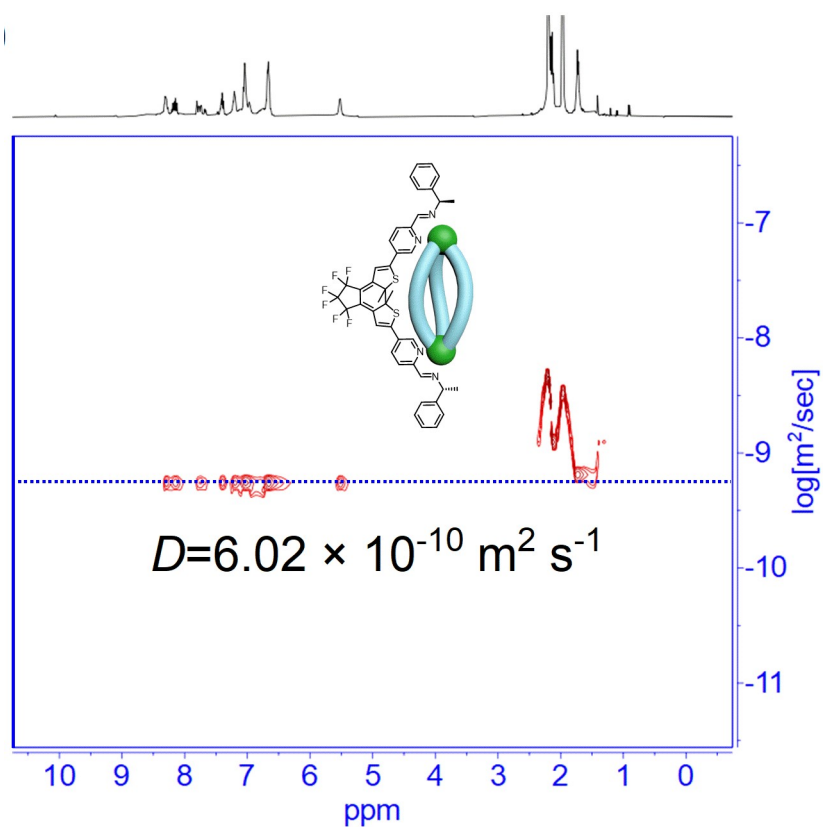$$D = 6.02 \times 10^{-10}\ \mathrm{m^2\ s^{-1}}$$

Fig. S9 DOSY spectrum of *c*-**cage**.

3.9 ESI-HRMS spectra of *o*-cage
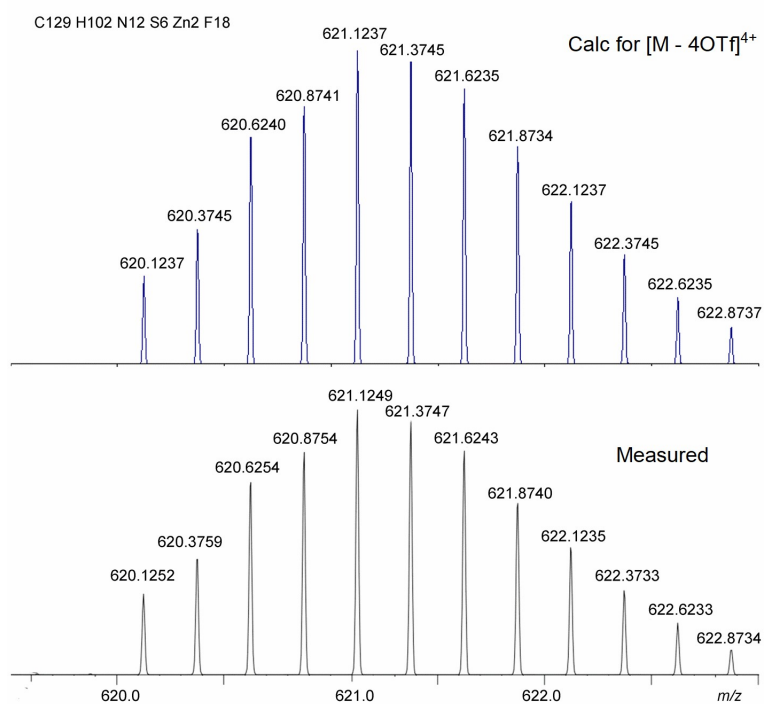
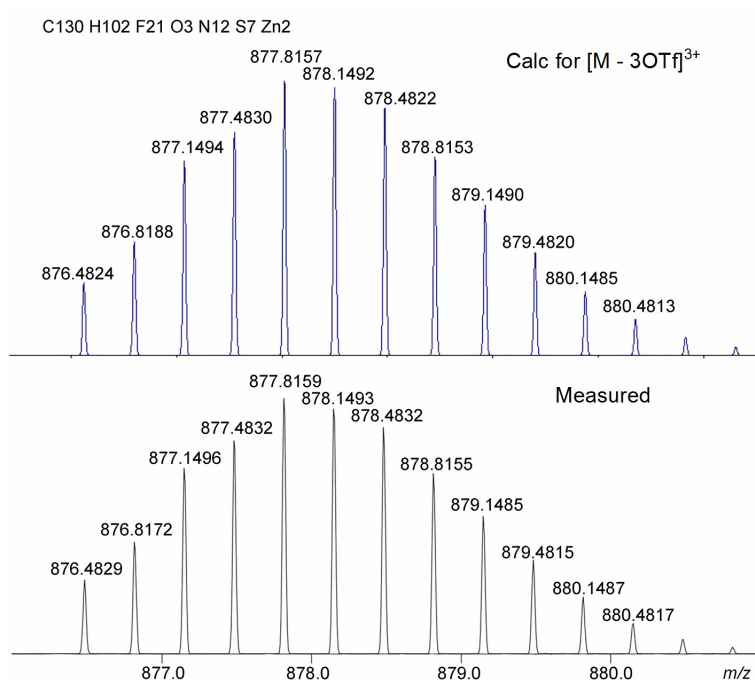**Fig. S10** ESI-HRMS spectrum of *c*-**cage** of [M - 4OTf]$^{4+}$, theoretical (top) and experimental (bottom).

C130 H102 F21 O3 N12 S7 Zn2

Calc for [M - 3OTf]$^{3+}$

877.8157
878.1492
878.4822
877.4830
878.8153
877.1494
879.1490
876.8188
879.4820
876.4824
880.1485
880.4813

877.8159
878.1493
878.4832
877.4832
878.8155
877.1496
879.1485
876.8172
879.4815
876.4829
880.1487
880.4817

Measured

877.0   878.0   879.0   880.0   *m/z*

Fig. S11 ESI-HRMS spectrum of *c*-**cage** of [M - 3OTf]$^{3+}$, theoretical (top) and experimental (bottom).

C131 H102 F24 O6 N12 S8 Zn2

Calc for [M - 2OTf]$^{2+}$

1391.7001
1391.1998
1392.1995
1390.7007
1392.7009
1390.2004
1393.1999
1389.7015
1393.7005
1389.2000
1394.1996
1394.7010

1391.7017
1391.2018
1392.2018
1390.7018
1392.7015
1390.2014
1393.2014
1389.7035
1393.7009
1389.2023
1394.2007
1394.7001

Measured

1389   1390   1391   1392   1393   1394   1395   *m/z*
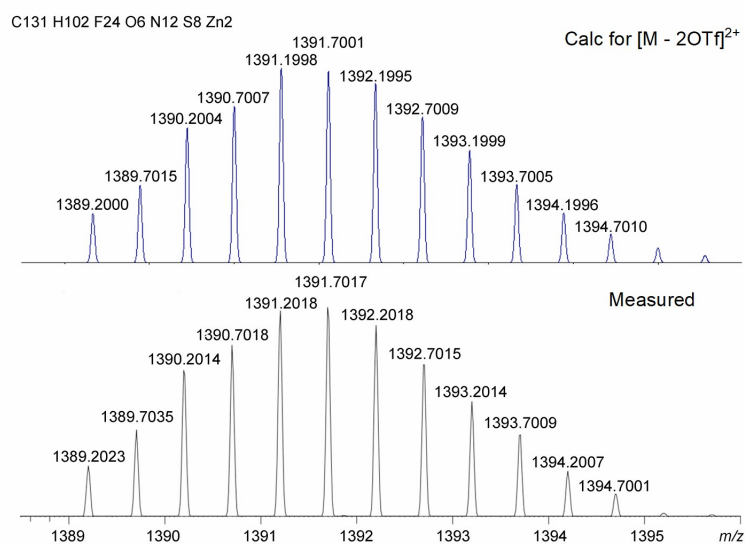
Fig. S12 ESI-HRMS spectrum of *c*-**cage** of [M - 2OTf]$^{2+}$, theoretical (top) and experimental (bottom).

4. Optimization and calculation of *S*-*c*-cage and *c*-cage

Density functional theory (DFT) geometry optimization calculations were performed on the three chiral isomers *S*-*RSS*, *S*-*RRS*, *S*-*SSS* isomers with M06-L functional and def2-SVP basis set, using Gaussian 16 C.01.[2] Relative energies of the same calculation level are shown in Table S1 and S2.

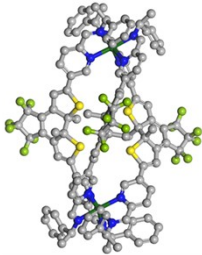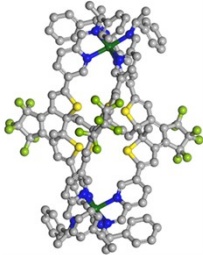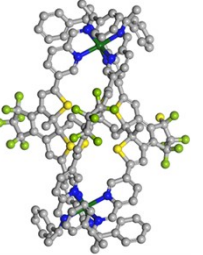**Table S1** Structure optimization and energy calculations of chiral metallacages by DFT calculation.
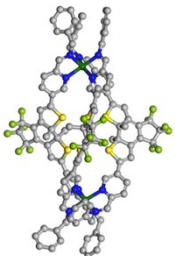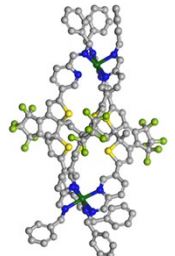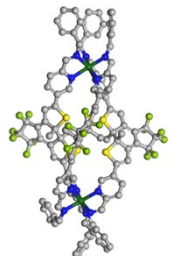
	(*S*)-phenethylamine-(*RRS*)-*c*-**cage**	(*S*)-phenethylamine-(*RSS*)-*c*-**cage**	(*S*)-phenethylamine-(*SSS*)-*c*-**cage**
Metallacage Structure			
E/Hartree	-13371.8926368	-13371.9013306	-13371.9033347
ΔE/kJ·mol^{-1}	28.09	5.26	0.00 (lowest)

Table S2 Structure optimization and energy calculations of achiral metallacages by DFT calculation.

	achiral (*RRS*)-*c*-**cage**	achiral (*RSS*)-*c*-**cage**	achiral (*SSS*)-*c*-**cage**
Metallacage Structure			
E/Hartree	-13136.1783499	-13136.1774699	-13136.1769284
ΔE/kJ·mol^{-1}	0.00	2.31	3.73

As shown in Table S1, for example, the (*S*)-phenethylamine-(*RSS*)-c-cage is depicted as (*S*)-(*RSS*) for simplicity. The energy sequence is (*S*)-(*RRS*) > (*S*)-(*RSS*) > (*S*)-(*SSS*), which can be attributed to the subtle induction effect from chiral amine to the DAE units. Among them, the (*S*-*SSS*) isomer has the lowest energy and is the most stable. If *S*-amine is used to construct the metal cage, the lower the proportion of *R*-c-DTE, the more stable it is. When compared with achiral metallacages *c*-**2** isomers in Table S2, we found that (RRS), (RSS), and (SSS) isomers have almost the equal energy, indicating the *S*-isomer of DTE units is preferentially induced when *S*-amine is used to construct the metallacages.

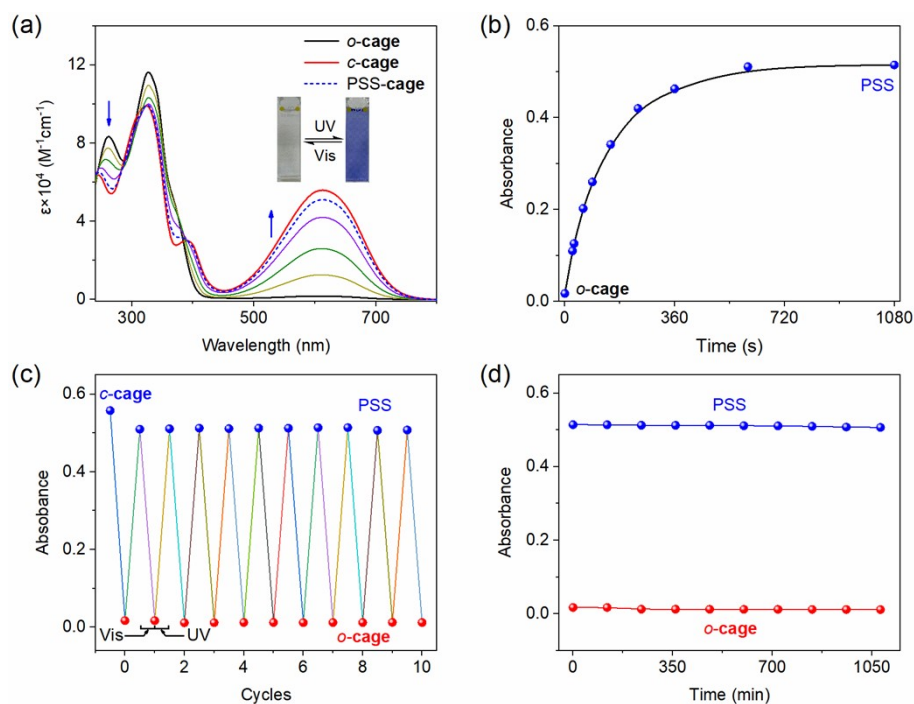# 5. Photoresponsive properties of metallacages

Fig. S13 (a) Absorption spectra of **cage** (1.0×10^{-5} M) in CH_3CN upon UV irradiation at 313 nm. (b) Absorption changes of **cage** along with time at 610 nm. (c) Absorption of *o*-**cage** ($\lambda = 610$ nm, $c = 1 \times 10^{-5}$ M) in CH_3CN upon irradiation of UV light ($\lambda = 313 \pm 10$ nm) and visible light ($\lambda > 510$ nm). (d) Decay curves of *o*-**cage** ($c = 1 \times 10^{-5}$ M, 298 K) at open- and PSS state upon irradiation of UV light ($\lambda = 313 \pm 10$ nm), monitored at absorption maximum ($\lambda = 610$ nm).

The photochromic behaviours were further investigated in metallacages. As found in Fig. S13a, *o*-**cage** displayed two intensive absorption bands at 260 and 340 nm. Upon UV light irradiation (313 ± 10 nm), the acetonitrile solution of the *o*-**cage** changed from colourless to blue with an increase in a broad peak at 450 – 770 nm, which can be attributed to the large π conjugate structure formation of closed-form. We calculated the photoconversion yield of 91.3% according to the absorption spectra. Alternating irradiation with UV (313 ± 10 nm) and visible light (> 510 nm) repeatedly switched the metallacages between ring-open and ring-closed forms, demonstrating remarkable fatigue resistance with no apparent degradation after 10 cycles (Fig. S13c). Furthermore, these cages have excellent thermal stability in both the open- and PSS, with no obvious decays for 1000 minutes at 298 K (Fig. S13d). These photochemistry results indicated that the responsive metallacages maintain excellent photochromic performance without obvious limitation by the metallacage framework.
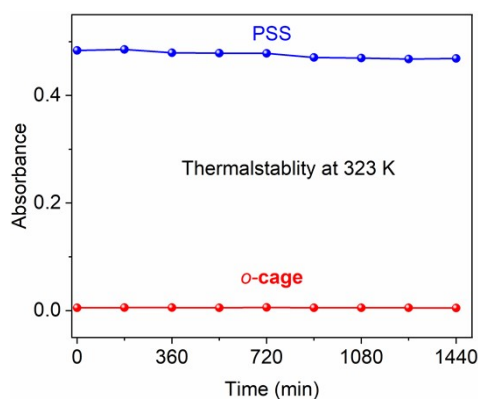

Fig. S14 Decay curves of *o*-**cage** ($c = 1 \times 10^{-5}$ M, 323 K) at open- and PSS state upon irradiation of UV light ($\lambda = 313 \pm 10$ nm), monitored at absorption maximum ($\lambda = 610$ nm).

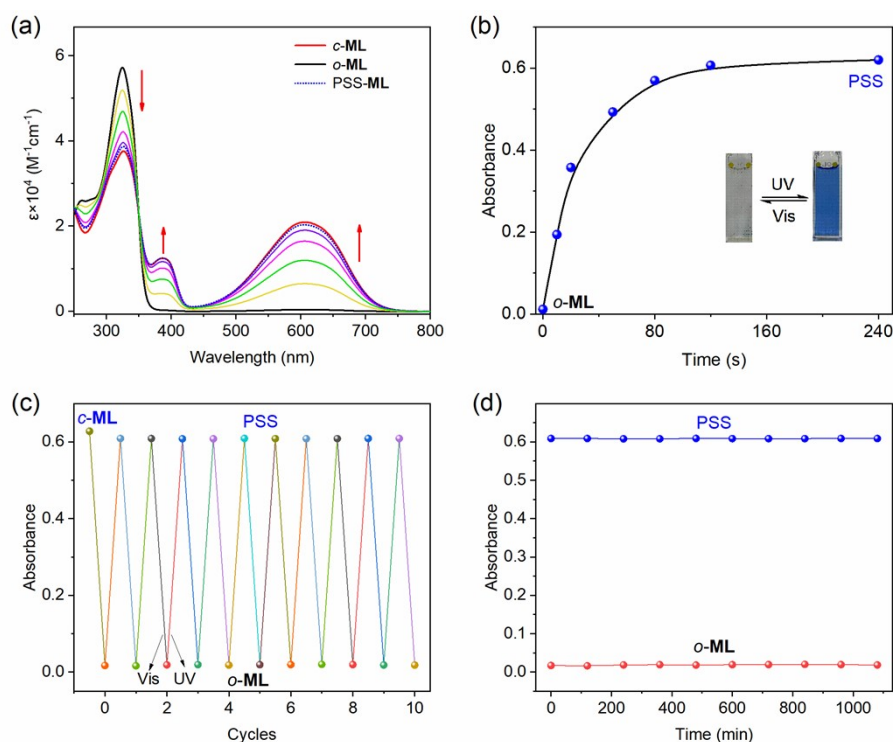# 6. Photoresponsive properties of free model ligands

Fig. S15 (a) Absorption spectra of **ML** (3.0×10^{-5} M) in CH$_3$CN upon UV irradiation at 313 nm. (b) Absorption changes of **ML** along with time at 605 nm. (c) Absorption of *o*-**ML** ($\lambda = 605$ nm, $c = 3 \times 10^{-5}$ M) in CH$_3$CN upon irradiation of UV light ($\lambda = 313 \pm 10$ nm) and visible light ($\lambda > 510$ nm). (d) Decay curves of *o*-**ML** ($c = 3 \times 10^{-5}$ M, 298 K) at open- and PSS state upon irradiation of UV light ($\lambda = 313 \pm 10$ nm), monitored at absorption maximum ($\lambda = 605$ nm).

The photochromic properties of free model ligands are the meaningful reference to evaluate performance of metallacages. As found in Fig. S15a, *o*-**ML** displayed an intensive absorption band at 325 nm. Upon UV light irradiation (313 ± 10 nm), the acetonitrile solution of the *o*-**ML** changed from colorless to blue with an increase in a broad peak at $450 - 770$ nm, which can be attributed to the large π conjugate structure formation of closed-form. We calculated the photoconversion yield of 94.1% according to the absorption spectra. Alternating irradiation with UV (313 ± 10 nm) and visible light (> 510 nm) repeatedly switched the model ligands between ring-open and ring-closed forms, demonstrating remarkable fatigue resistance with no apparent degradation after 10 cycles (Fig. S15c). Furthermore, these cages have excellent thermal stability in both the open- and PSS, with no obvious decays for 1000 minutes at 298 K (Fig. S15d). The detail comparation is mentioned in main text.

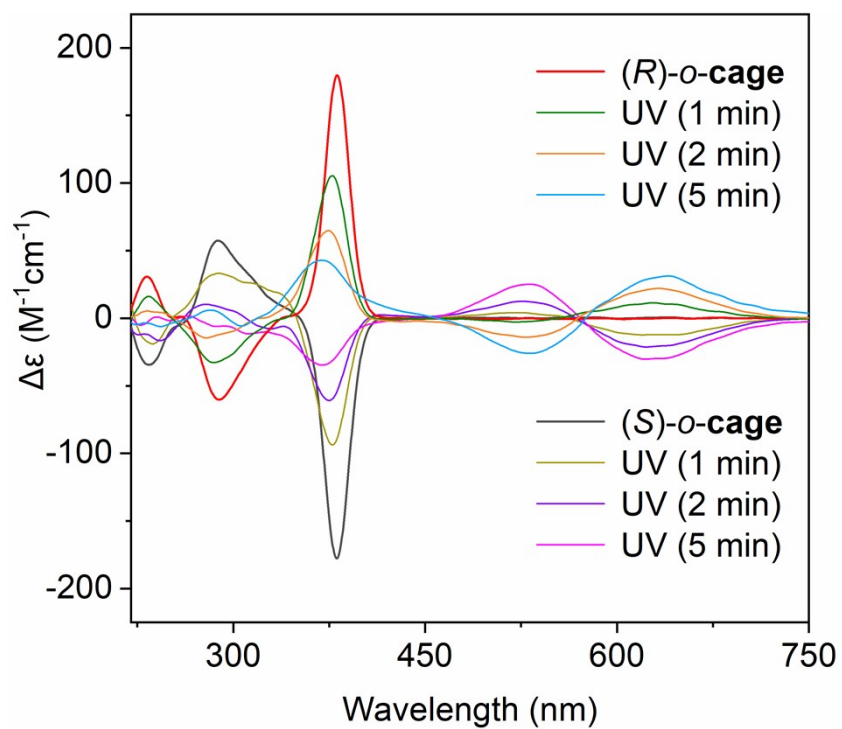# 7. Circular dichroism modulation of metallacages

Fig. S16 CD spectrum of (*R/S*)-*o*-**cage** ($c_{(R)}$=3.4 × 10^{-5} M, $c_{(S)}$=3.3 × 10^{-5} M) in CH_3CN upon UV irradiation at 313 nm.

8. Determination of photochromic Quantum Yields

For the photocyclization quantum yields of *o*-**cage** and *o*-**ML** according to the reported method.[3] Commercial compound **BTF6** was used as reference for measuring the intensity of light source. The detailed procedure: i) 2 mL of *o*-**BTF6** (1×10^{-4} M) in hexane solution was irradiated until PSS state; ii) measuring the absorbance at 517 nm before and after irradiation; iii) Under the same light intension, measuring the absorbance at 595 nm for *o*-**cage** and 605 nm for *o*-**ML** before and after irradiation at 313 nm.
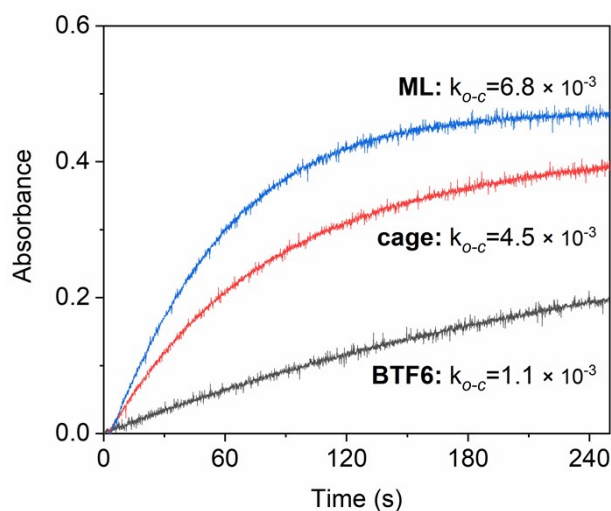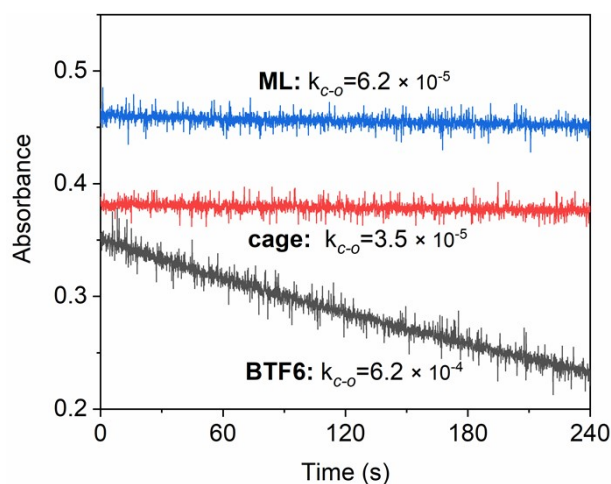

Fig. S17 The absorbance changes of ring-open isomers **BTF6** ($\lambda = 517$ nm, $c = 1 \times 10^{-4}$ M in hexane), *o*-**ML** ($\lambda = 610$ nm, $c = 3 \times 10^{-5}$ M in CH$_3$CN), *o*-**cage** ($\lambda = 595$ nm, $c = 1 \times 10^{-5}$ M in CH$_3$CN) upon UV irradiation at 313 nm.

For the photocycloreversion quantum yields of *c*-**cage** and *c*-**ML**. The detailed procedure: i) 2 mL of *PSS*-**BTF6** (1×10^{-4} M) in hexane solution. was irradiated until open state; ii) measuring the absorbance at 517 nm before and after irradiation; iii) Under the same light intension, measuring the absorbance at 595 nm for *c*-**cage** and 605 nm for *c*-**ML** before and after irradiation at 545 nm.

Fig. S18 The absorbance changes of ring-closed isomers **BTF6** ($\lambda = 517$ nm, c $= 1 \times 10^{-4}$ M in hexane), *c*-**ML** ($\lambda = 610$ nm, c $= 3 \times 10^{-5}$ M in CH$_3$CN), *c*-**cage** ($\lambda = 595$ nm, c $= 1 \times 10^{-5}$ M in CH$_3$CN) upon visible irradiation at 545 nm.

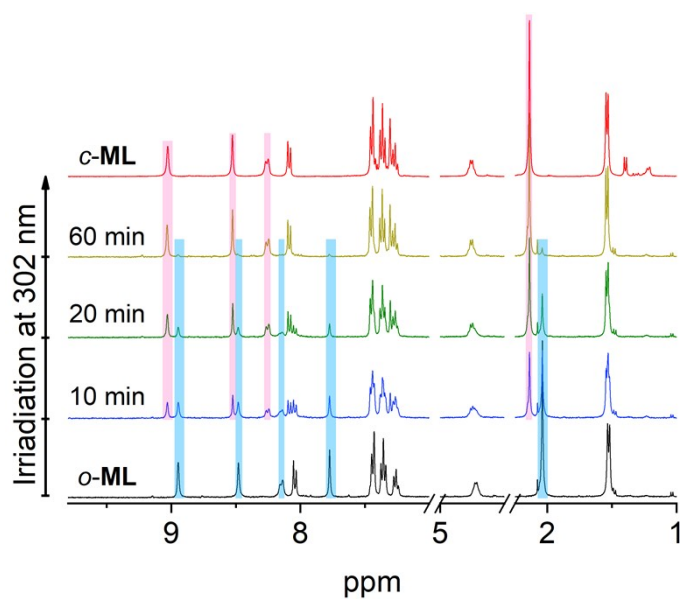# 9. Isomerization monitoring of the free model ligand by ^{1}H NMR

Fig. S19 Partial ^{1}H NMR (400 MHz, DMSO-d_6, 293 K) spectra of the structural photoconversion of ML from the ring-open to the ring-closed upon UV irradiation ($\lambda = 302 \pm 10$ nm).

According to the ^{1}H NMR spectrum of the free model ligand, we observed a series of clear proton peaks belong to *o*-**ML**. When exposed to the UV light ($\lambda = 302 \pm 10$ nm), we found the transformation from *o*-**ML** to *c*-**ML**, without any intermediate product. We utilized this one-to-one transformation mechanism to compare and investigate the isomerization of metallacages.
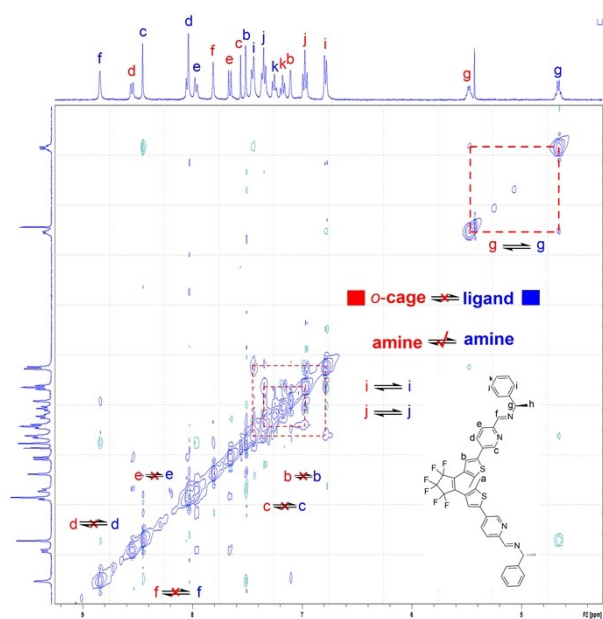
10. EXSY spectrum of metallacages and free ligands

Fig. S20 EXSY spectrum (400 MHz, CD$_3$CN/CDCl$_3$, 298 K, mixture time = 600 ms) of the *o*-**cage** and model ligand.
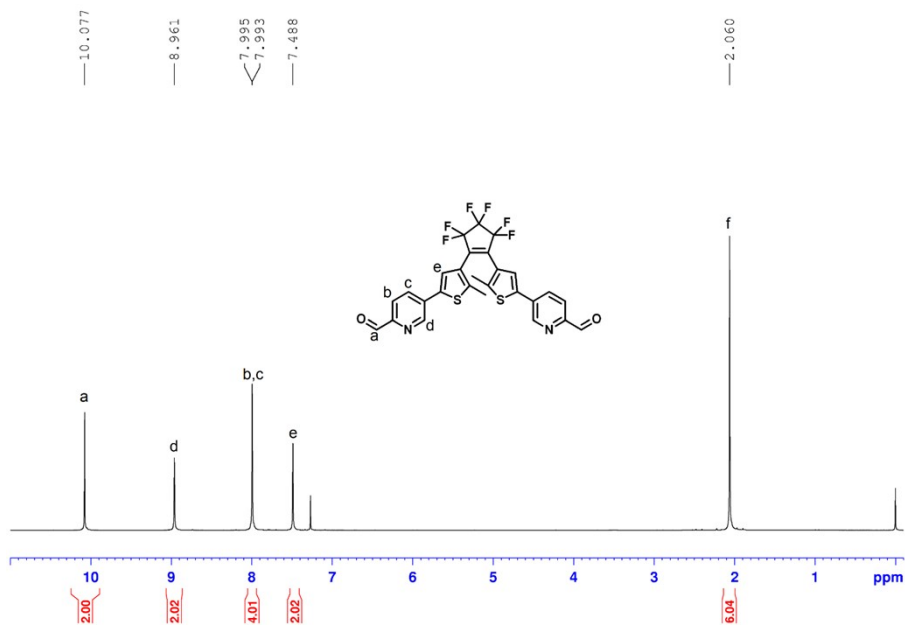
11. Characterization of ligands and achiral metallacages

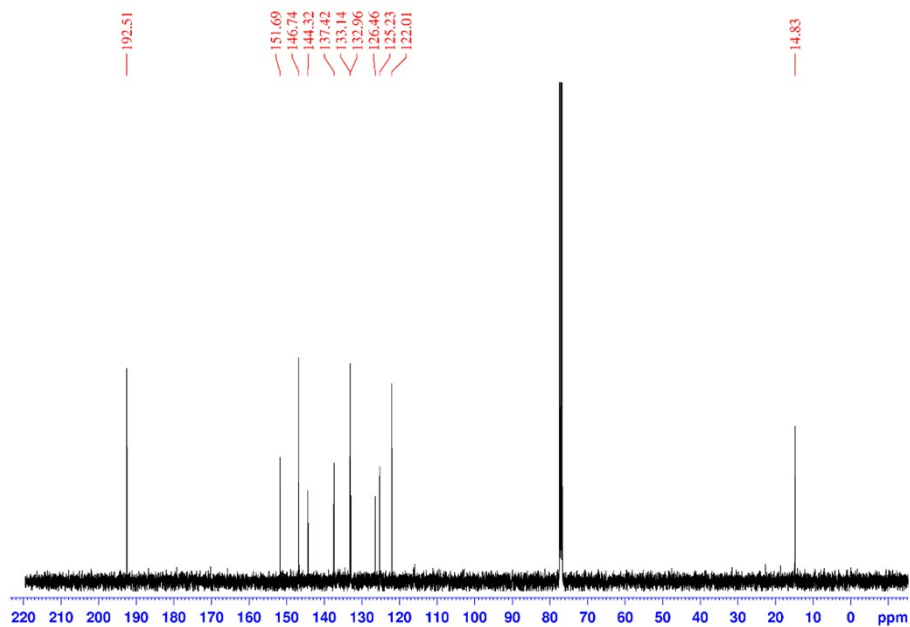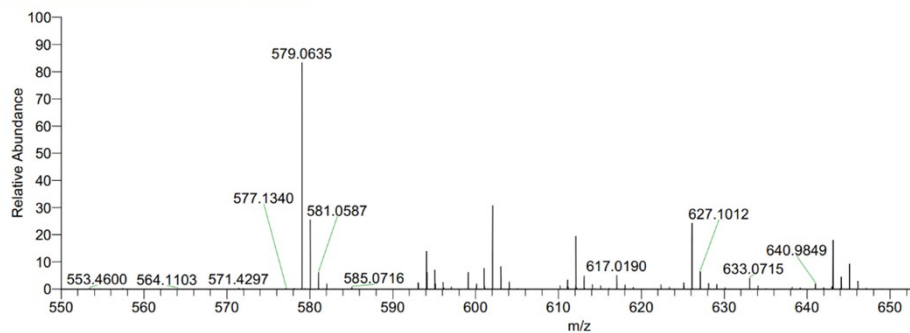**Fig. S21** ^{1}H NMR (400 MHz, CDCl$_3$, 293 K) spectrum of ligand *o*-**PA**.

Fig. S22 ^{13}C NMR (100 MHz, CDCl$_3$, 293 K) spectrum of ligand *o*-**PA**.

m/z	Intensity	Relative	Theo. Mass	Delta (ppm)	Composition
579.0635	11861346.0	100.00	579.0630	0.51	$C_{27}H_{17}O_2N_2F_6S_2$

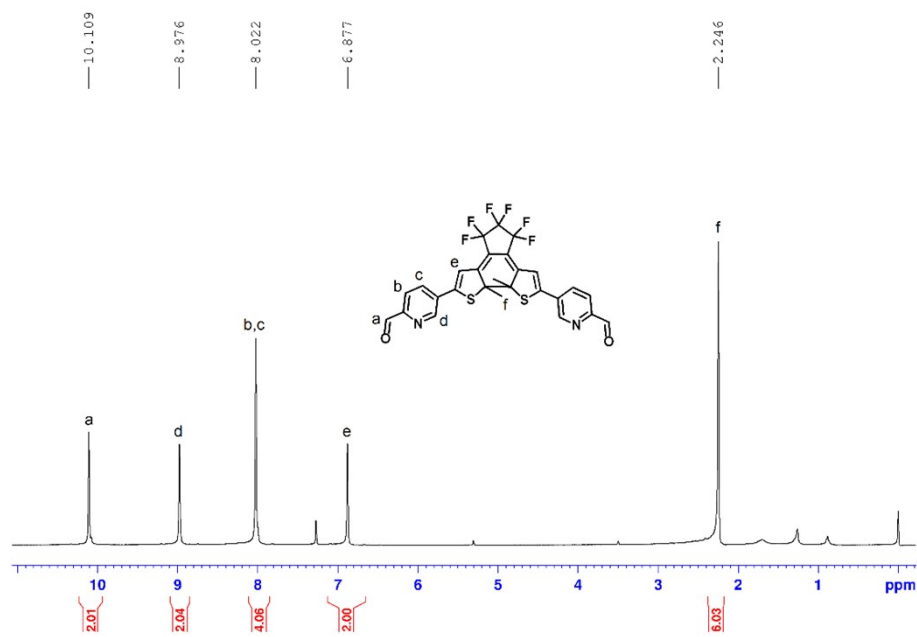**Fig. S23** HRMS spectrum of ligand *o*-**PA**.

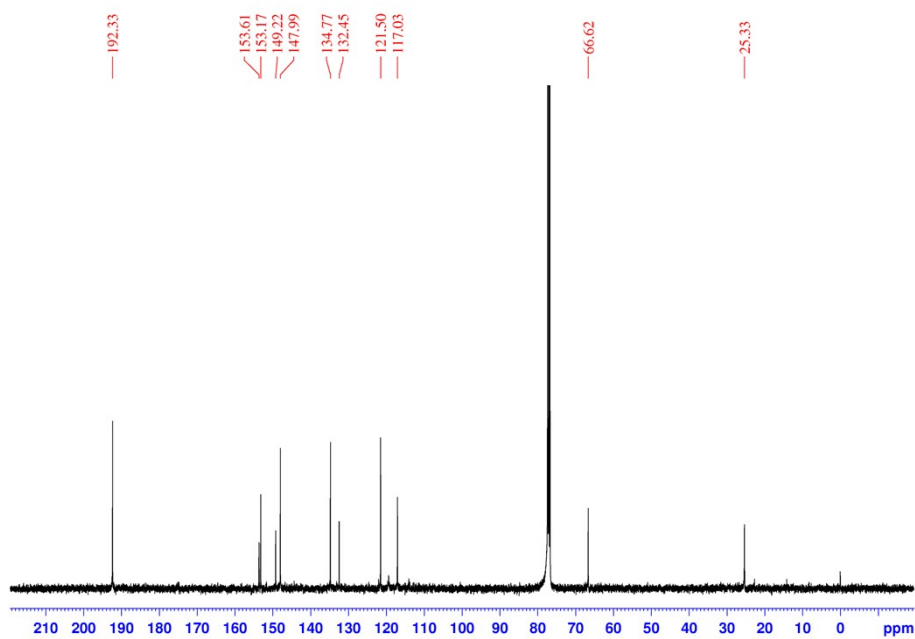**Fig. S24** ^{1}H NMR (400 MHz, CDCl$_3$, 293 K) spectrum of ligand *c*-**PA**.

Fig. S25 ^{13}C NMR (100 MHz, CDCl$_3$, 293 K) spectrum of ligand *c*-**PA**.
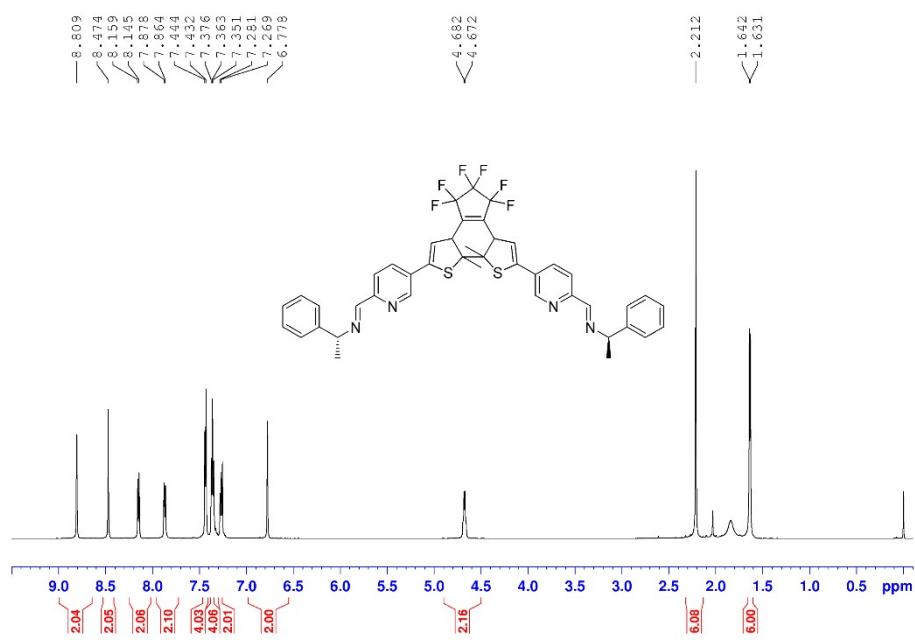

Fig. S26 ^{1}H NMR (600 MHz, CDCl$_3$, 293 K) spectrum of model ligand *c*-**ML**.
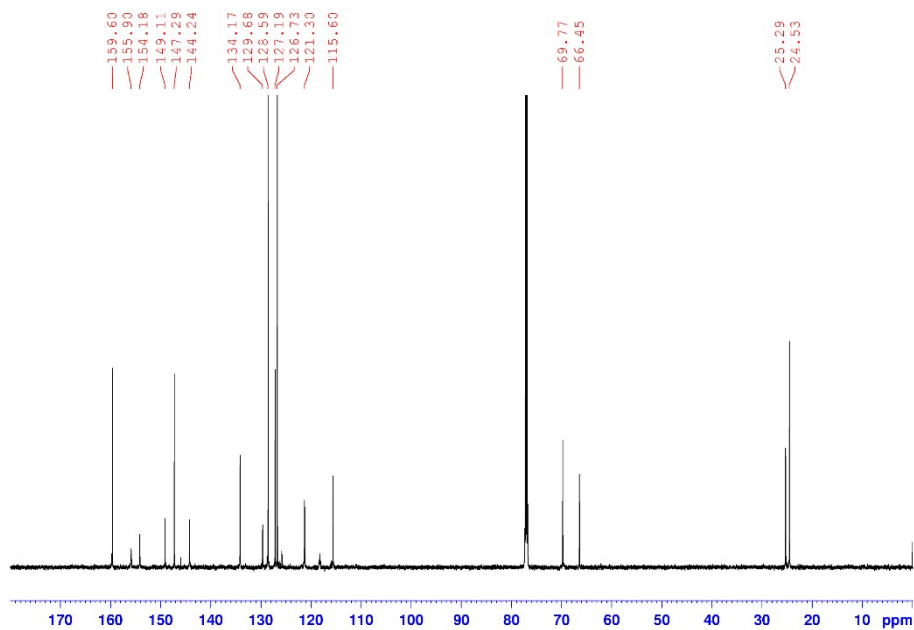
Fig. S27 ^{13}C NMR (150 MHz, CDCl$_3$, 293 K) spectrum of model ligand *c*-**ML**.
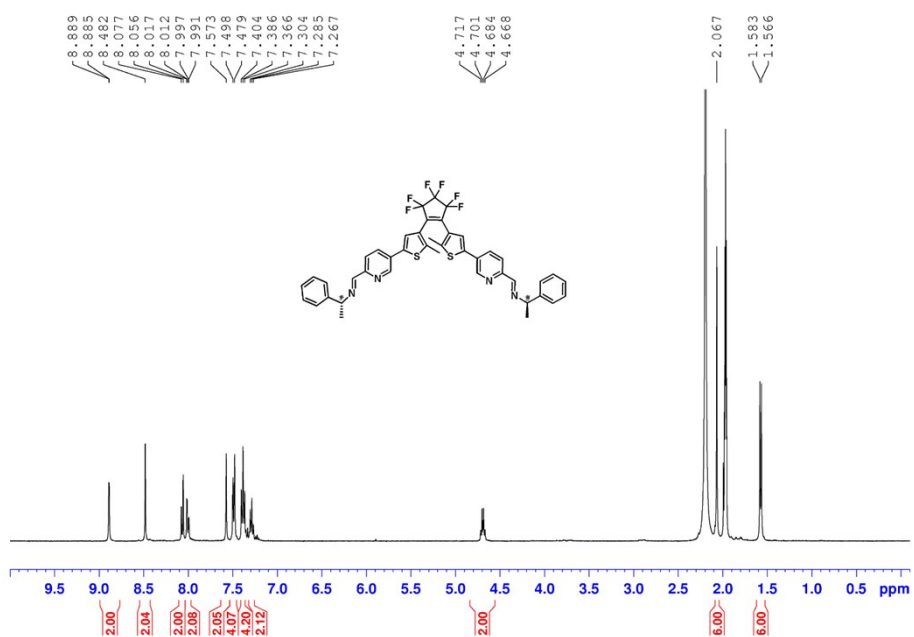

Fig. S28 ^{1}H NMR (400 MHz, CD$_3$CN, 293 K) spectrum of model ligand *o*-**ML**.

Single Mass Analysis
Tolerance = 10.0 PPM / DBE: min = -1.5, max = 50.0
Element prediction: Off
Number of isotope peaks used for i-FIT = 3
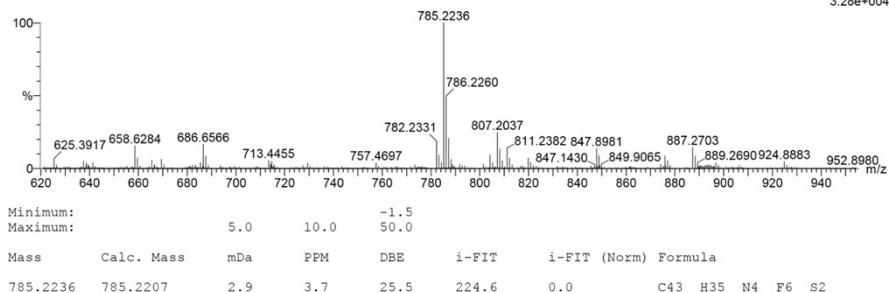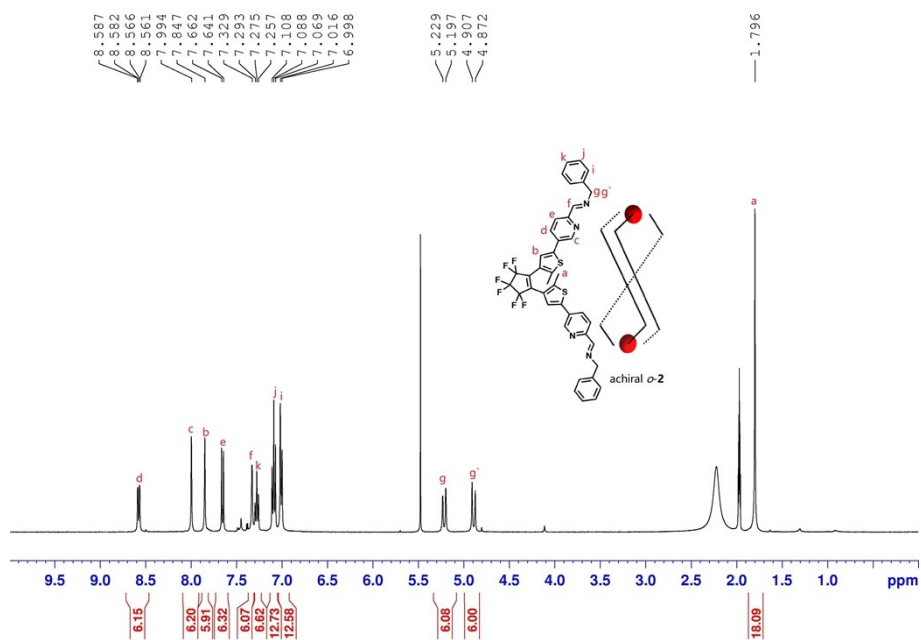
Monoisotopic Mass, Even Electron Ions
412 formula(e) evaluated with 1 results within limits (up to 50 best isotopic matches for each mass)
Elements Used:
C: 0-43 H: 0-35 N: 0-4 F: 0-6 S: 0-2 Br: 0-2

WH-ZHU
ZW-GSM-9231 272 (3.118) Cm (256:273)   1: TOF MS ES+
                                                                3.28e+004

Minimum:				-1.5			
Maximum:		5.0	10.0	50.0			
Mass	Calc. Mass	mDa	PPM	DBE	i-FIT	i-FIT (Norm)	Formula
785.2236	785.2207	2.9	3.7	25.5	224.6	0.0	C43 H35 N4 F6 S2

Fig. S29 ESI-HRMS spectrum of model ligand *o*-**ML**.

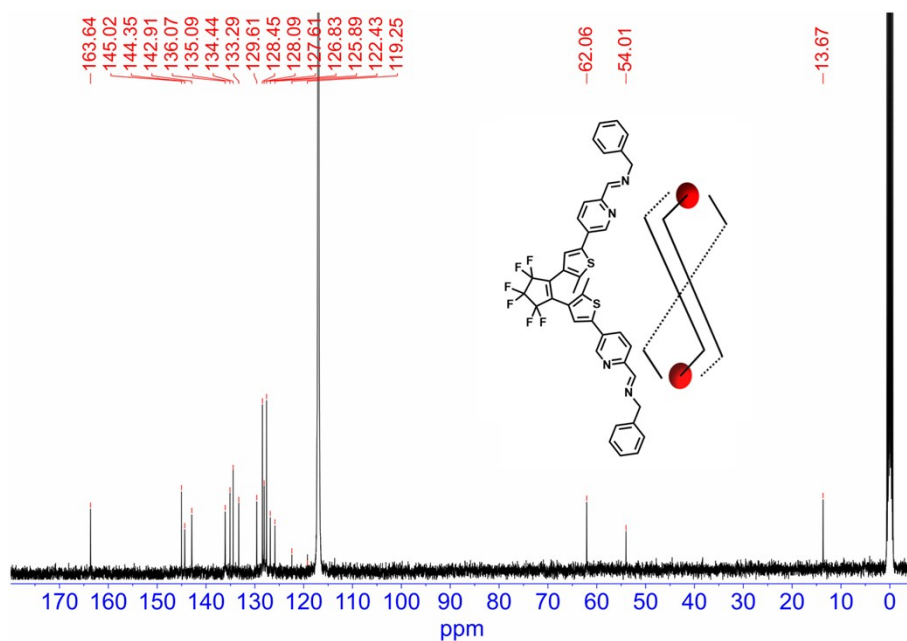**Fig. S30** ¹H NMR (400 MHz, CD₃CN, 293 K) spectrum of achiral *o*-**2**.

Fig. S31 ^{13}C NMR (100 MHz, CD$_3$CN, 293 K) spectrum of achiral *o*-**2**.
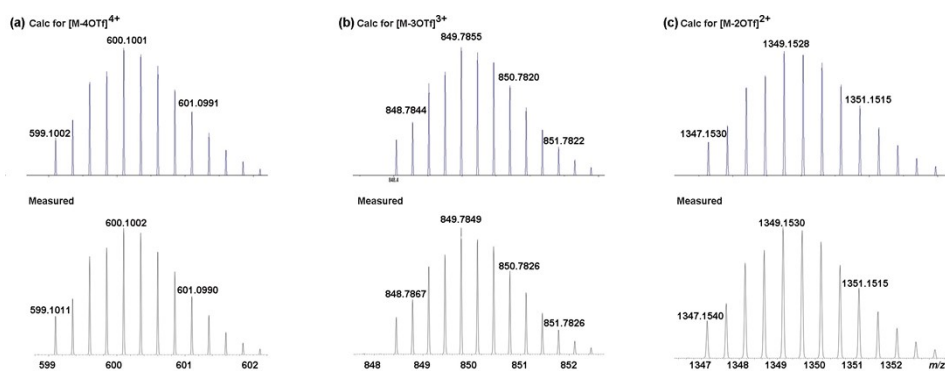

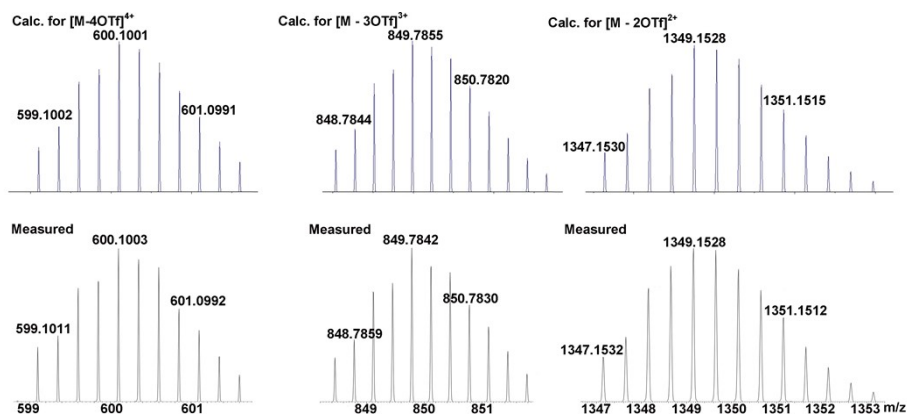**Fig. S32** ESI-HRMS spectrum of *o*-**2**

Fig. S33 ESI-HRMS spectrum of *c*-**2**

12. References

1   J. W. Chung, S.-J. Yoon, S.-J. Lim, B.-K. An and S. Y. Park, *Angew. Chem. Int. Ed.*, 2009, **48**, 7030.
2   Gaussian 16, Revision C.01, Frisch, M. J.; Trucks, G. W.; Schlegel, H. B.; Scuseria, G. E.; Robb, M. A.; Cheeseman, J. R.; Scalmani, G.; Barone, V.; Petersson, G. A.; Nakatsuji, H.; Li, X.; Caricato, M.; Marenich, A. V.; Bloino, J.; Janesko, B. G.; Gomperts, R.; Mennucci, B.; Hratchian, H. P.; Ortiz, J. V.; Izmaylov, A. F.; Sonnenberg, J. L.; Williams-Young, D.; Ding, F.; Lipparini, F.; Egidi, F.; Goings, J.; Peng, B.; Petrone, A.; Henderson, T.; Ranasinghe, D.; Zakrzewski, V. G.; Gao, J.; Rega, N.; Zheng, G.; Liang, W.; Hada, M.; Ehara, M.; Toyota, K.; Fukuda, R.; Hasegawa, J.; Ishida, M.; Nakajima, T.; Honda, Y.; Kitao, O.; Nakai, H.; Vreven, T.; Throssell, K.; Montgomery, J. A., Jr.; Peralta, J. E.; Ogliaro, F.; Bearpark, M. J.; Heyd, J. J.; Brothers, E. N.; Kudin, K. N.; Staroverov, V. N.; Keith, T. A.; Kobayashi, R.; Normand, J.; Raghavachari, K.; Rendell, A. P.; Burant, J. C.; Iyengar, S. S.; Tomasi, J.; Cossi, M.; Millam, J. M.; Klene, M.; Adamo, C.; Cammi, R.; Ochterski, J. W.; Martin, R. L.; Morokuma, K.; Farkas, O.; Foresman, J. B.; Fox, D. J. Gaussian, Inc., Wallingford CT, **2016**.
3   S. Fukumoto, T. Nakashima and T. Kawai, *Angew. Chem. Int. Ed.*, 2011, **50**, 1565.